ELSEVIER

Chemical Physics 268 (2001) 21–34

Chemical Physics

www.elsevier.nl/locate/chemphys

On the Bayesian approach to calculating time correlation functions in quantum systems; reaction dynamics and spectroscopy

Goran Krilov, Eunji Sim, B.J. Berne *

Department of Chemistry, Columbia University, 3000 Broadway, New York, NY 10027, USA

Received 12 January 2001

Abstract

We assess the current status, advantages and limitations of the numerical analytic continuation approach to computing time correlation functions in large many-body quantum systems characteristic of condensed phase chemical processes. We determine the quantum correlation function as a function of complex time, and use its analytic properties to select a suitable contour in the complex time plane along which the function can be evaluated efficiently by stochastic simulation methods. The simulation data are then used to obtain the values of the correlation function along the real-time axis through a maximum entropy numerical analytic continuation procedure. This approach is used to compute the dynamical properties of several condensed phase processes including vibrational relaxation lineshapes and canonical reaction rates. We discuss how to improve the accuracy of the numerical analytic continuation methods.

1. Introduction

Many properties of complex chemical systems that are both important and accessible experimentally are of time-dependent nature. Some examples include quantities such as transport coefficients, inelastic light and neutron scattering cross-sections, dipole relaxation times and reaction rates. The experimental methods used to measure these quantities share a common characteristic, that is they monitor the response of the system to a perturbation caused by a weak external field. In this regime, the dynamics of the system is adequately described by the linear response theory, which implies that the measured dynamic properties can be expressed in terms of two-point time correlation functions of the corresponding dynamic operators [1].

Molecular dynamics (MD) [2,3] methods, based on integrating equations of motion, have been successfully used to compute time correlation functions in classical systems. However, in many chemical systems of interest, quantum effects play a significant role in the dynamics, and classical treatment is not adequate for the accurate determination of time-dependent properties. It is thus highly desirable to develop a method for computing time-correlation functions of an arbitrary many-body quantum system.

A general quantum time correlation function is given by

* Corresponding author. Fax: +1-212-854-7454.
E-mail address: berne@chem.columbia.edu (B.J. Berne).

0301-0104/01/$ - see front matter
PII: S0301-0104(01)00287-7

$$C(t) = \langle A(t)B(0)\rangle = \tfrac{1}{Z}\mathrm{Tr}\left(\mathrm{e}^{-\beta H}\mathrm{e}^{\mathrm{i}Ht/\hbar}A\mathrm{e}^{-\mathrm{i}Ht/\hbar}B\right), \quad (1)$$

where A and B are quantum mechanical operators corresponding to measurable observables, H is the Hamiltonian of the system, and $\beta = 1/kT$ is the inverse temperature, and Z is the canonical partition function. Evaluating the above requires simulating the time evolution of a finite temperature many-body quantum mechanical system, which has proven to be a formidable problem. Due to large system size, basis-set methods and wave-packet propagation techniques often used to solve the time-dependent Schroedinger equation for small systems cannot be used directly. This leaves path integral methods as the only feasible alternative. However, in contrast to equilibrium properties, computation of time-dependent canonical averages using path integrals requires evaluation of multidimensional integrals over rapidly oscillating exponentials due to the presence of real-time propagators. Therefore, the number of paths that must be summed to obtain a statistically converged result grows exponentially with the propagation time, which leads to inefficiency and inevitable failure of stochastic methods based on importance sampling. This phenomenon is known as the "sign problem", and is the primary obstacle to using computer simulations to compute quantum time-correlation functions. It has been pointed out by Feynman that this problem is NP complete and he suggested that quantum computers could offer a solution [4].

Several approximate approaches have been developed in an effort to avoid the above difficulty. Mixed quantum/classical methods [5–12] use numerically exact methods to propagate a few relevant quantum degrees of freedom, while the rest of the system is treated classically. Semiclassical methods [13–18] treat all degrees of freedom within the semiclassical approximation. The centroid molecular dynamics (CMD) [19–21] method provides an approximate means of computing approximate time correlation functions of operators which are linear in position and momentum for very large systems. The method is exact for purely harmonic systems, and gives physically reasonable results in cases which do not deviate substantially from this limit.

Other approaches seek to suppress the sign problem in evaluating real-time integrals. These include methods based on the use of stationary phase filtering [22–27], optimized reference systems [28–30], and more recently renormalization techniques [31–34]. While these methods introduce great advantages over direct sampling of real-time path integrals, they are limited to either certain types of systems or relatively modest system sizes.

In this paper we address an alternative approach, based on exploiting analytic properties of quantum time correlation functions. In general, the quantum time correlation functions are evaluated using path integral methods along a suitable finite contour in the complex time plane, and these data is used to obtain the values along the real time axis through a numerical analytic continuation procedure. This approach possesses several desirable properties: it allows the entire system to be treated fully quantum mechanically, without making a priori approximations; it is computationally feasible for large systems; it is applicable to arbitrary many-body systems. As such, it seems to offer a viable path to a general method for simulation of quantum dynamics, which would be capable of handling large systems with strongly anharmonic interactions, which is characteristic of chemical reactions in liquids.

For all the cases in this paper, the environment or bath is described by harmonic oscillators and the system and bath are bilinearly coupled. Therefore following Zwanzig [35] and Caldeira and Leggett [36] the total Hamiltonian is given by

$$H(x,\{x_\alpha\},p,\{p_\alpha\}) = H_\mathrm{s}(x,p) + \sum_\alpha \left(\frac{p_\alpha^2}{2m_\alpha} + \frac{1}{2}m_\alpha\omega_\alpha^2 x_\alpha^2\right) - x\sum_\alpha c_\alpha x_\alpha, \quad (2)$$

where $H_\mathrm{s}(x,p)$ is system Hamiltonian and coordinate and momentum (x_α, p_α) correspond to a harmonic mode of the environment with mass m_α and frequency ω_α. We describe the environment in terms of the spectral density function $J(\omega)$

$$J(\omega) = \frac{\pi}{2}\sum_\alpha \frac{c_\alpha^2}{m_\alpha\omega_\alpha}\delta(\omega-\omega_\alpha). \quad (3)$$

Although the numerical analytic continuation approach presented in this review is applicable to a general condensed phase system we use the harmonic bath model to demonstrate the method since there are often exact solutions available.

In Section 2 we discuss the analytic properties of quantum time correlation functions by considering several complex time contours leading to various forms of correlation functions related to each other through analytic continuation. In Section 3 we outline the maximum entropy (ME) procedure used to perform the analytic continuations numerically. We present several applications of the method in calculating vibrational relaxation lineshapes and quantum reaction rates in Sections 4 and 5 respectively. We conclude with Section 6.

2. Complex time contours and analytic continuation relationships

In order to investigate the analytic properties of the time correlation function, one can consider a more general form, which is a function of a complex time variable $z = t - \mathrm{i}\tau$,

$$C(z) = \langle A(z)B(0)\rangle. \tag{4}$$

For the remainder of this paper, we limit our discussion to autocorrelation functions, namely $A = B$. Baym and Mermin have shown [37] that if the function $C(z)$ is known along the imaginary time axis, that is the contour $z = -\mathrm{i}\tau$, for $0 < \tau < \beta\hbar$ (shown in Fig. 1), one can infer its values along the real time axis (contour $z = t$ in Fig. 1) through an analytic continuation procedure.

In general, for the purpose of expressing the analytic continuation relationships it is convenient to introduce $I(\omega)$, the power spectrum of $C(z)$, such that

$$C(z) = \frac{1}{2\pi}\int_{-\infty}^{\infty} \mathrm{d}\omega\, \mathrm{e}^{\mathrm{i}\omega z} I(\omega). \tag{5}$$

To illustrate the utility of the above results, consider a position basis representation of $C(z)$:

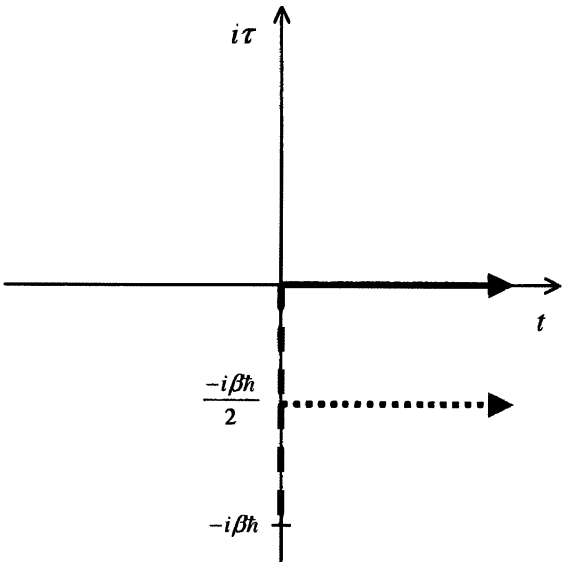

Fig. 1. A schematic representation of the contours in the complex time plane along which $C(z)$ is evaluated. The solid line is the $z = t$ contour corresponding to the real-time correlation function, the dotted line is the $z = t + \mathrm{i}\beta$ is the contour along which the symmetrized time correlation function is evaluated, and the dashed line shows the $z = -\mathrm{i}\tau$, the imaginary time contour which is bounded by $0 < \tau < \beta\hbar$.

$$C(z) = \frac{1}{Z}\int \mathrm{d}x\,\mathrm{d}x'\,\mathrm{d}x'' A(x'')A(x)\langle x|^{-\beta H}|x'\rangle \times \langle x'|\mathrm{e}^{\mathrm{i}Hz/\hbar}|x''\rangle\langle x''|\mathrm{e}^{-\mathrm{i}Hz/\hbar}|x\rangle, \tag{6}$$

where we have used one dimensional notation and assumed A to be diagonal in x for clarity. The determination of $C(z)$ along the real-time contour, $z = t$ requires the evaluation of integrals over pairs of forward and backward real-time paths, connecting x and x'' as well as x'' and x to compute matrix elements $\langle x'|\mathrm{e}^{\mathrm{i}Ht/\hbar}|x''\rangle$ and $\langle x''|\mathrm{e}^{-\mathrm{i}Ht/\hbar}|x\rangle$. One should note that these paths have no positive definite weights due to the presence of real-time propagators with purely imaginary phases. As a result, stochastic importance sampling methods cannot be used to evaluate these integrals directly. In contrast, evaluating $C(z)$ along the imaginary time axis, $z = -\mathrm{i}\tau$, requires one to compute the product $\langle x'|\mathrm{e}^{H\tau/\hbar}|x''\rangle\langle x''|\mathrm{e}^{-H\tau/\hbar}|x\rangle$. This involves integrals over imaginary time paths which have positive definite weights, and can hence be

efficiently computed by Monte Carlo sampling even for very large systems. In other words, while it is very difficult to evaluate $C(z)$ along $z = t$, it can be readily computed along $z = -i\tau$. $C(-i\tau)$, which is often called the imaginary time correlation function, is related to $C(t)$ through

$$C(t) = \frac{1}{2\pi}\int_{-\infty}^{\infty} d\omega\, e^{i\omega t} I(\omega), \tag{7}$$

and

$$C(-i\tau) = \int_{-\infty}^{\infty} d\omega\, e^{-\omega\tau} I(\omega). \tag{8}$$

To compute $C(t)$ from $C(-i\tau)$ it is necessary to obtain $I(\omega)$ by performing an inverse transform of Eq. (8). Typically, the value of $C(-i\tau)$ is available from computer simulations at several values of τ with finite statistical errors. In this case, the inverse transform must be performed numerically, which is a highly unstable operation. Inverse Laplace transformation of noisy data is an ill-posed problem due to the highly singular nature of the Laplace kernel. As a consequence, specialized methods need to be used in order to control the numerical instability.

Methods based on maximum entropy and singular value decomposition have been employed in this context for a range of dynamical problems, including lattice models [38], and an electron solvation [39,40], vibrational relaxation [41,42], adsorbate vibrational lineshape [43], and quantum reaction rates [44]. In all the cases it was found that very accurate data for $C(-i\tau)$ are necessary in order to obtain satisfactory results. Even then, the unstable nature of the inverse Laplace transform due to the singular nature of the kernel results in correlation functions that are accurate over relatively short times, so the method was limited to cases in which quantum correlations decay on that time scale.

A possible way of alleviating this problem is to evaluate $C(z)$ along a different contour in the complex time plane [45], one which would be related to the $z = t$ contour through a more stable numerical analytic continuation. We consider one such contour, namely $z = t - i\beta\hbar/2$. The related correlation function, $G(t) \equiv C(t - i\beta\hbar/2)$

$$G(t) = \left\langle A\left(t - \frac{i\beta\hbar}{2}\right)B(0)\right\rangle = \frac{1}{Z}\mathrm{Tr}\left(e^{iH(t+i\beta\hbar/2)/\hbar}Ae^{-iH(t-i\beta\hbar/2)/\hbar}B\right) \tag{9}$$

is known as the symmetrized time correlation function and has been considered before by Berne and co-workers [46,47]. They showed that the resulting path integrals that need to be computed to evaluate the matrix elements of complex time propagators in the above expression involve integrals over paths with complex weights, the real parts of which can be used as a weight in Monte Carlo sampling. Furthermore, the cancellation of phases in forward and backward complex time paths should reduce the severity of the sign problem, allowing one to compute $G(t)$ by computer simulations up to moderate but short times for arbitrary large systems.

On the other hand, to determine $I(\omega)$ from $G(t)$ one needs to numerically invert

$$G(t) = \frac{1}{\pi}\int_0^{\infty} d\omega \cos(\omega t) e^{-\beta\hbar\omega/2} I(\omega), \tag{10}$$

which is expected to be much more stable than the inverse Laplace transform required in Eq. (8) due to a better behaving kernel. One thus evaluates $G(t)$ by simulation up to a finite value of time t_c and then performs numerical analytic continuation to invert Eq. (10) and obtain $C(t)$.

It should be noted that in both cases, the simulation data will be available only at a finite number of values of z, and each of those will be known within a statistical uncertainty. Thus in both cases, there will be a range of solutions consistent with a set of simulation data. In the next section, we describe the maximum entropy method, which provides a means of selecting the most probable one among various possible solutions. We have used simulation data for $C(z)$ evaluated at various combinations of $z = -i\tau$ and $z = t - i\beta\hbar/2$ contours and tested the approach for several systems of interest, with the results presented in the following sections.

3. Maximum entropy method

The maximum entropy (ME) [48,49] inversion method has been shown to be useful for many problems in which there are incomplete and noisy data. The method itself requires only the knowledge of the transformation which relates the data and the solution. Furthermore, prior knowledge about the solution is included in a logically consistent fashion. As such, ME is ideally suited for solving ill-posed mathematical problems. A particularly important class of such problems involves inverting integral equations of the type

$$D(\tau) = \int \mathrm{d}\omega K(\tau,\omega)A(\omega), \tag{11}$$

where $K(\tau,\omega)$ is a singular kernel. Eqs. (7) and (8) relating the real-time correlation functions evaluated along various complex time contours belong to this class. If the data set $D(\tau)$ is noisy and incomplete, the solution $A(\omega)$, also referred to as the map, cannot be determined uniquely. Maximum entropy criteria provide a method for determining the most probable inversion consistent with the data. This method is based on Bayesian inference. Typically, the data are known only at a discrete set of points $\{\tau_i\}$, and we likewise seek a solution at a discrete set of points $\{\omega_j\}$. The maximum entropy method selects a solution which maximizes the probability of the map $\mathbf{A}$ given a data set $\mathbf{D}$, known as the posterior probability [38,48]

$$\mathscr{P}(\mathbf{A}|\mathbf{D}) \propto \exp(\alpha S - \chi^2/2) = \mathrm{e}^{Q}. \tag{12}$$

Here χ^2 is the standard mean squared deviation from the data

$$\chi^2 = \sum_{j,k}\left(D_j - \sum_l K_{jl}A_l\right)[C^{-1}]_{jk}\left(D_k - \sum_l K_{kl}A_l\right), \tag{13}$$

where C_{jk} is the covariance matrix

$$C_{jk} = \frac{1}{M(M-1)}\sum_{l=1}^{M}\left(\langle D_j\rangle - D_j^{(l)}\right)\left(\langle D_k\rangle - D_k^{(l)}\right) \tag{14}$$

with M being the number of measurements.

S is the information entropy, the form of which is axiomatically chosen to be

$$S = \sum_k \Delta\omega\left(A_k - m_k - A_k \ln\frac{A_k}{m_k}\right). \tag{15}$$

In this formulation the entropy is measured relative to a default model $m(\omega)$ which can contain prior information about the solution and α is a positive regularization parameter.

Finding a map $\mathbf{A}$ which maximizes the posterior probability is a maximization problem in N variables, where N is the number of points $\{\omega_k\}$ at which the solution is evaluated. The solution obtained in this way is still conditional on the arbitrary parameter α, which can be interpreted as a regularization parameter controlling the smoothness of the map. Large values of α lead to a result primarily determined by the entropy function and hence the default model. Small α in turn lead to a map determined mostly by the χ^2 and thus to a closer fitting of the data. The principal drawback is that, along with the data, the errors would be fit as well. The optimal value of α is determined by the L-curve method [50,51]. The value of α is selected by constructing a plot of $\log[-S(\mathbf{A})]$ vs. $\log\chi^2$. This curve has a characteristic L-shape, and the corner of the L, or the point of maximum curvature, corresponds to the value of α which is the best compromise between fitting the data and obtaining a smooth solution. We note that there are other methods for selecting α [38,49], however we found that the L-curve method is adequate for our purpose.

In our studies thus far we have used a flat default map, which satisfies a known sum rule, such as the integral over $A(\omega)$. Other choices of $m(\omega)$ and their effect on the quality of the results will be the subject of future investigation.

4. Dipolar time correlation functions and spectral lineshapes

We have computed spectral lineshapes of the position autocorrelation functions for several bound systems, i.e., $A(x) = B(x) = x$ in Eq. (1) for system coupled bilinearly to harmonic bath [39].

These are in turn related to the photon absorption cross section given by

$$\sigma(\omega) = \left(\frac{4\pi}{\hbar c}\right)\omega\left(1 - \mathrm{e}^{-\beta\hbar\omega}\right)I(\omega). \tag{16}$$

We discuss two systems namely a harmonically bound electron and a proton in a quartic well. Details of the study are in our previous work [42]. In addition to being a classic model for vibrational relaxation processes, the harmonic oscillator system coupled to harmonic bath is the only many body system for which exact solutions for quantum position autocorrelation functions are available. In particular, it was shown that the classical photon absorption cross-section, obtained in closed form by solving the generalized Langevin equation [52] is equal to the quantum one [53] and this system was studied previously by analytic continuation of the imaginary time correlation function [41].

For the harmonic system potential, symmetrized real time correlation data was included up to $t = \beta\hbar/2 = 0.125$ a.u., which is the same as the imaginary time range, since $C(-\mathrm{i}\tau)$ is symmetric around $\tau = \beta\hbar/2$ and the data for $\beta\hbar/2 < \tau < \beta\hbar$ do not provide any new information. The ME inversions were performed using imaginary time data alone, symmetrized time correlation function alone and the combination of the two [42]. The results for power spectra and the real parts of the corresponding position autocorrelation functions are shown in Fig. 2(a) and (b) in comparison with exact results. The same procedure was then performed using $G(t)$ data for real-time up to $t = 0.25$ a.u. (computed by MC according to the prescrip-

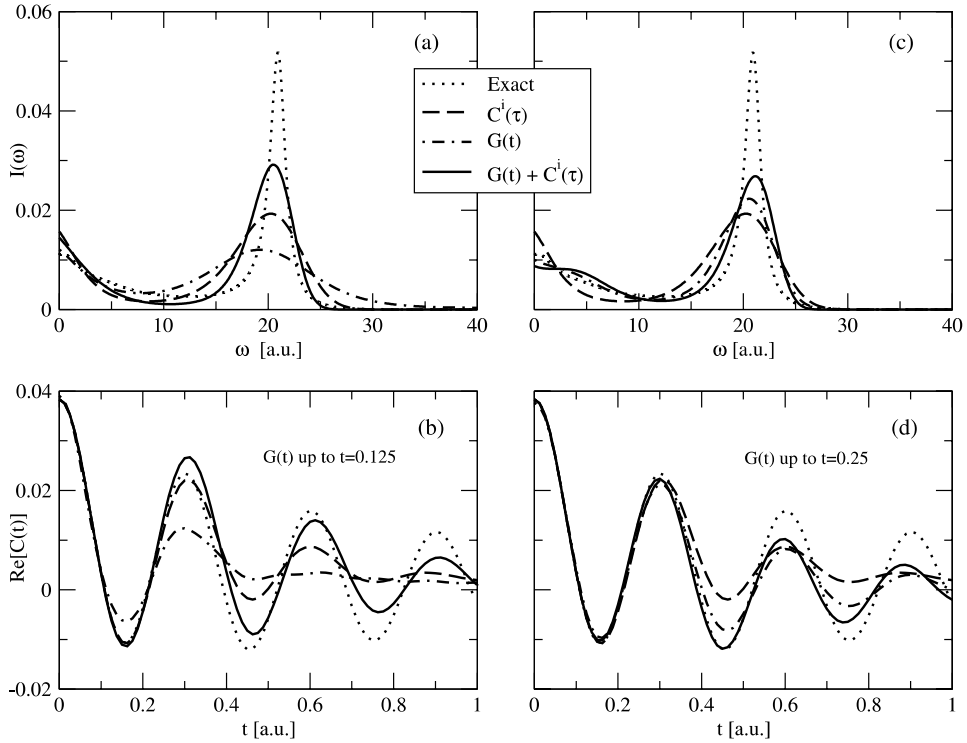

Fig. 2. Analytic continuation results for a harmonic oscillator coupled to a harmonic environment. In (a) we show the power spectra and in (b) the real parts of the corresponding real-time position correlation functions obtained by ME continuation of imaginary time data (broken line), symmetrized time correlation data (dot-dashed line) and the combination of the two (solid line) in comparison with the exact result (dotted line). The symmetrized time correlation function data was included up to $t = 0.5$ a.u. In (c) and (d) we show the same results using symmetrized time correlation data up to $t = 1.0$ a.u. This figure is reproduced from Fig. 4 of Ref. [42].

tion of Refs. [42,47,54]) with the results shown in Fig. 2(c) and (d). Including symmetrized time correlation function data leads to an improvement. The analytic continuation using imaginary time data results in a real-time correlation function accurate to $t = 0.3$ a.u., or on the order of $\beta\hbar$. This is superior to the results using only $G(t)$ data in the first case, but in the second case, continuation using longer time symmetrized correlation function data (up to $t = 0.25$ a.u.) yields a real-time correlation function accurate to $t = 0.45$ a.u. In particular, the low frequency portion of the spectrum is well reconstructed. This behavior is not unexpected, as the power spectrum of $G(t)$ is related to $I(\omega)$ through $G(\omega) = e^{-\beta\hbar\omega/2} I(\omega)$, it is thus primarily determined by the low frequency region of $I(\omega)$.

Similar behavior was observed in a highly anharmonic system, namely a quartic oscillator interacting with a dissipative environment [42]. For this case we used $G(t)$ data up to $t = 790$ a.u. ($0.5\beta\hbar$). The resulting power spectra are shown in Fig. 3(a) and the real parts of the corresponding real-time correlation functions in Fig. 3(b). Due to the presence of the anharmonic potential, the full quantum dynamics cannot be obtained exactly. However, it is possible to compute the symmetrized correlation functions up to intermediate times (several multiples of $\beta\hbar$) using a non stochastic approach based on exact evaluation of integrals in the discrete variable representation of path integrals. These are shown in Fig. 3(c) in comparison with the symmetrized time correlation functions computed from the power spectra in Fig. 3(a) using Eq. (10).

A systematic improvement can be observed as the time domain of the simulated $G(t)$ data is extended. We used ME analytic continuation to compute the real-time correlation functions from symmetrized correlation functions, for several sets of $G(t)$ with increasing cutoff time t_c. The results for the power spectra, and the real-time and symmetrized time correlation functions computed from the former are shown in Fig. 4(a)–(c) respectively at temperature $T = 200$ K. The improvement is evident in comparison with exact $G(t)$ results in Fig. 4(c), which is accurately reproduced as the cutoff time is increased. It should be noted that the gain in the time range (i.e. the range over which the analytically continued real-time results are accurate compared to the cutoff time up to which the $G(t)$ data are available) appears to increase with increasing cutoff time. As the computational effort for real-time path integrals increases exponentially with time, this is particularly significant, as it allows one to compute accurate quantum time correlation functions for significantly longer times than that could be attained by direct simulation of $G(t)$.

To summarize, in both cases, the real time correlation functions obtained using the combination of imaginary and symmetrized time correlation data in the analytic continuation process were accurate over much longer times than those obtained from imaginary time data alone. In particular, we observed that as the time domain (i.e. the cutoff time up to which simulation data is available) of the symmetrized time correlation data used in analytic continuation is lengthened, the range over which the real-time correlation functions are accurate increases substantially. Moreover, for longer time domains, the symmetrized time correlation data dominates in the ME inversion scheme, and combination with imaginary time data leads to the same result as using $G(t)$ data on its own. This clearly shows that expanding the time domain leads to a more stable inversion.

In contrast to analytic continuation utilizing only imaginary time correlation data, analytic continuation using the symmetrized time correlation function can be systematically improved by increasing the real-time cutoff. This is particularly evident in results for the quartic oscillator in Fig. 4, where using increasing values of the cutoff time for the $G(t)$ data leads to real-time correlation functions that are accurate over progressively longer times.

5. Quantum reaction rate constants

Rabani et al. [44] and Sim et al. [54] have applied short time analytic continuation to the calculation of quantum reaction rate constants. Following Miller et al. [55], the Boltzmann averaged

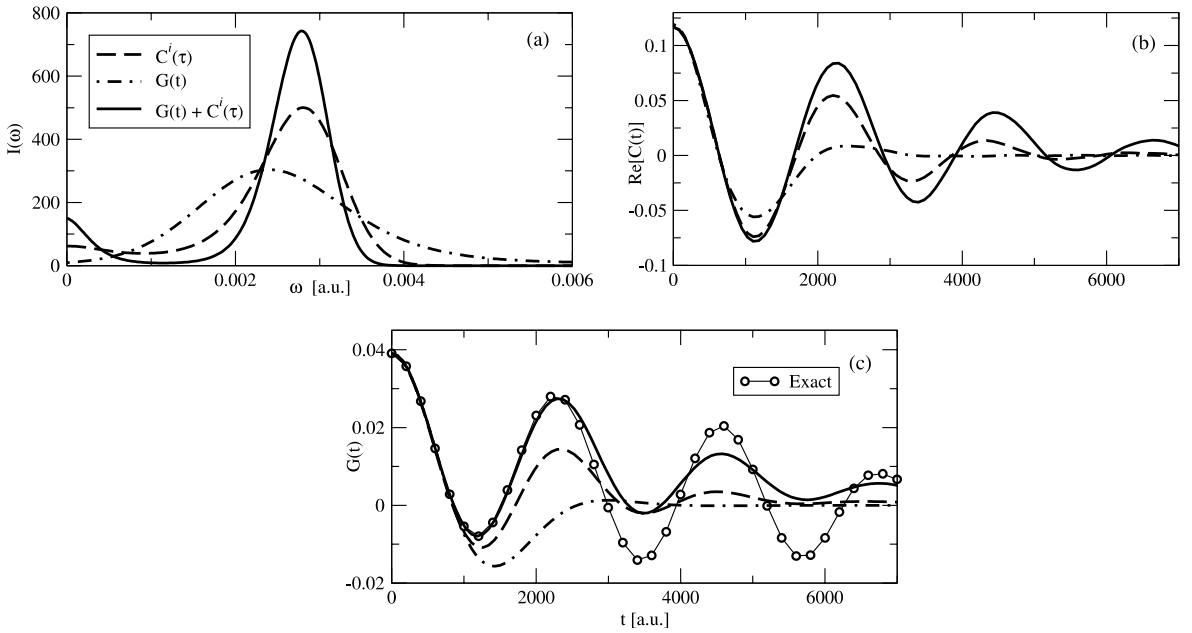

Fig. 3. Analytic continuation results for a quartic oscillator coupled to a harmonic environment at the temperature of 200 K. The symmetrized time correlation function data was included up to $t = 790$ a.u. In (a) we show the power spectra and in (b) the real parts of the corresponding real-time position correlation functions computed by ME continuation of imaginary time data (broken line), symmetrized time correlation data (dot-dashed line) and the combination of the two (solid line). In (c) we show the symmetrized correlation functions calculated from the power spectra in (a) in comparison with the exact result (empty circles). This figure is reproduced from Fig. 5 of Ref. [42].

quantum mechanical canonical rate constant is given by

$$k = \frac{Z}{Z_r}\int_0^\infty \mathrm{d}t\, C_F(t), \tag{17}$$

where $C_F(t)$ is a flux autocorrelation function

$$C_F(t) = \tfrac{1}{Z}\mathrm{Tr}[\hat{F}\mathrm{e}^{-\lambda H}\mathrm{e}^{\mathrm{i}\hat{H}t/\hbar}\hat{F}\mathrm{e}^{-\mathrm{i}\hat{H}t/\hbar}\mathrm{e}^{-(\beta-\lambda)H}]. \tag{18}$$

Here $\hat{F}$ is the symmetrized flux operator

$$\hat{F} = \frac{1}{2m_s}[\hat{p}_s\delta(\hat{s}) + \delta(\hat{s})\hat{p}_s], \tag{19}$$

and, for the sake of simplicity, the dividing surface through which the reactive flux is measured is located at $s = 0$. The rate constant expression in Eq. (17) was shown to be invariant to the value of λ ($0 \leqslant \lambda \leqslant \beta$) [55]. Since the correlation function is an even function of time, one can change the integration range and the rate is given by

$$k = \frac{1}{2}\int_{-\infty}^{\infty} \mathrm{d}t\, C_F(t) \tag{20}$$

for clarity, from this point forward, $C_F(t)$ includes the partition function ratio prefactor. One can then define a frequency dependent rate constant $k(\omega)$ [44],

$$k(\omega) = \frac{1}{2}\int_{-\infty}^{\infty} \mathrm{d}t\, \mathrm{e}^{\mathrm{i}\omega t} C_F(t) \tag{21}$$

such that the zero frequency value of $k(\omega)$ corresponds to the rate constant in Eq. (20).

For the purpose of obtaining the rate constants, the two complex contours described in Section 2 were used. The choice of the value of $\lambda = \beta/2$ in Eq. (18) leads to a symmetric form of the flux autocorrelation function [54–56]

$$G_F(t) = \tfrac{1}{Z}\mathrm{Tr}[\hat{F}\mathrm{e}^{\mathrm{i}\hat{H}t_c^*/\hbar}\hat{F}\mathrm{e}^{-\mathrm{i}\hat{H}t_c/\hbar}]. \tag{22}$$

$t_c = t - \mathrm{i}\beta\hbar/2$ is a complex time that arises from combining the time evolution operator with the

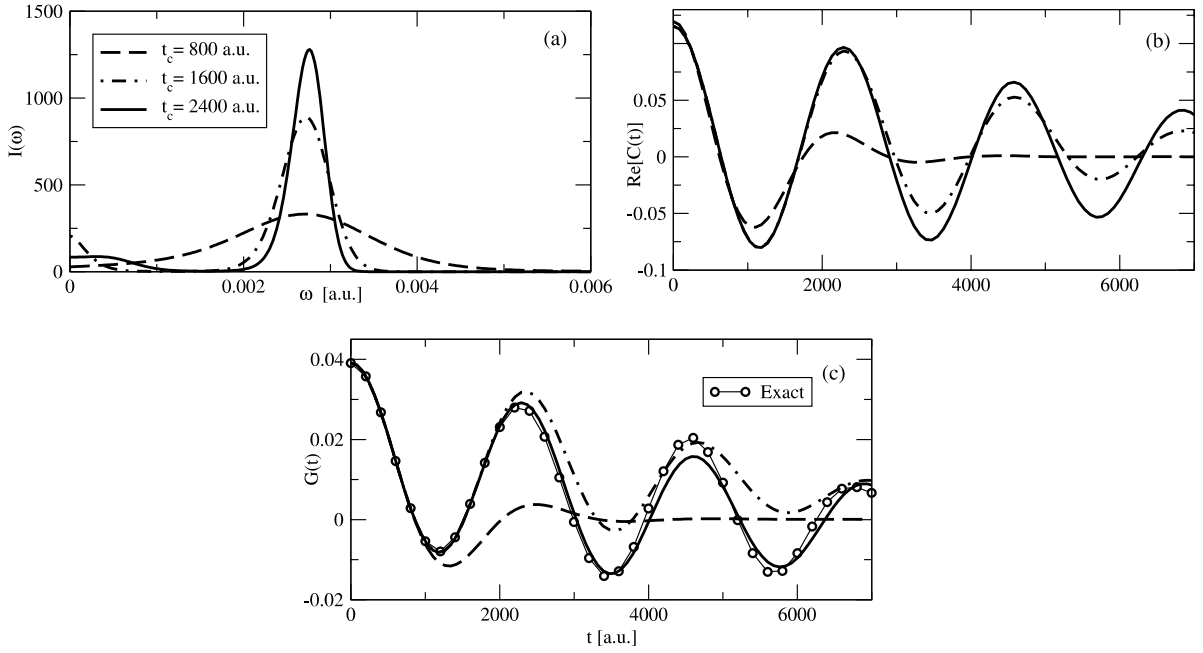

Fig. 4. Analytic continuation results for a quartic oscillator coupled to a harmonic environment at the temperature of 200 K. In (a) we show the power spectra and in (b) the real parts of the corresponding real-time position correlation functions computed by ME continuation of symmetrized time correlation function data computed by simulation up to the cutoff time $t_c = 800$ a.u. (broken line), $t_c = 1600$ a.u. (dot-dashed line) and $t_c = 2400$ a.u. (solid line). In (c) we show the symmetrized correlation functions calculated from the power spectra in (a) in comparison with the exact result (empty circles). This figure was reproduced from Fig. 7 of Ref. [42].

Boltzmann operator. Z and Z_r denote the total canonical partition function and the reactant side partition function, respectively, such that

$$\frac{Z}{Z_r} = \frac{\mathrm{Tr}[e^{-\beta E}]}{\mathrm{Tr}[e^{-\beta E}\hat{h}_r]} \tag{23}$$

with $\hat{h}_r$ being the reactant side projection operator. In order to relate the frequency dependent rate to the short-time symmetrized flux autocorrelation data Eq. (21) was inverted

$$G_F(t) = \frac{1}{\pi}\int_{-\infty}^{\infty} d\omega\, e^{-i\omega t} k(\omega). \tag{24}$$

Then the replacement $t \to -i\tau$ in Eq. (24) gives [44]

$$C_F(-i\tau) = \frac{1}{\pi}\int_{-\infty}^{\infty} d\omega\, e^{-\omega\tau} k(\omega), \tag{25}$$

where t, $\tau \geqslant 0$, $C_F(-i\tau)$ being the imaginary time flux autocorrelation function. Unlike the real time flux autocorrelation function, it is straightforward to obtain the imaginary time flux autocorrelation function using PIMC simulations even for a many-body system. Analytic continuation was performed by inverting the integral equation to obtain $k(\omega)$. This inversion is possible only if $C_F(-i\tau)$ is analytic over the desired range of τ [37]. It turns out that for $\lambda = 0$ the imaginary time flux autocorrelation function is not analytic at $\tau = 0$, which is the reason for introducing the parameter λ with a small positive value.

The numerical analytic continuation method can thus be used to compute the rate from either finite-time $G_F(t)$ by inverting Eq. (24) or alternatively from $C_F(-i\tau)$ by inverting Eq. (25). We give examples of rate constants that were obtained by using both approaches.

5.1. Double-well coupled to a harmonic bath

We model a typical proton transfer reaction by a double well bilinearly coupled to a harmonic bath.

The harmonic bath model was chosen to allow comparison of the results obtained by our method with those obtained from exact quantum mechanical calculations [56]. The two cases studied include a high barrier model with a wide spectral density labeled DW1, and a lower barrier model with a narrower spectral density labeled DW2. The rate constant was studied as a function of the friction constant as well as the temperature.

Fig. 5 shows several typical reactive flux correlation functions with $\lambda = \beta/2$ obtained by ME numerical analytic continuation of the simulation data available up to $t = \beta\hbar$ (left side of the vertical dotted line) [54]. The reactive flux correlation function $R(t)$ is a time integral of the symmetrized flux autocorrelation function $G_{\mathrm{F}}(t)$. Note that there are dynamically important events that occur after the time $t = \beta\hbar$ and the results for all three different friction constants well illustrate that the long time behavior of crossing and recrossing events is successfully predicted by the short time analytic continuation procedure.

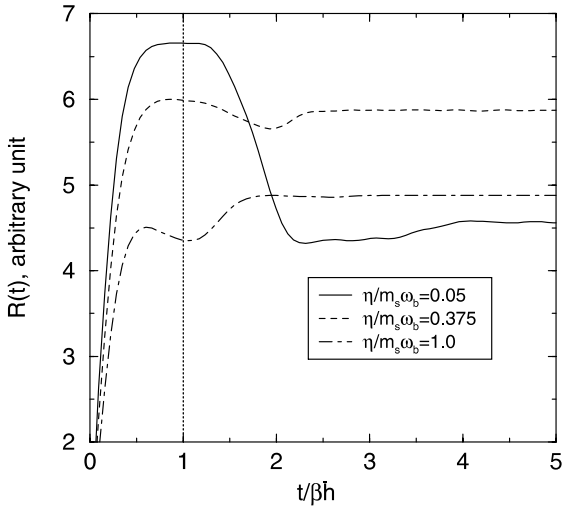

Fig. 5. Analytically continued results of reactive flux correlation functions, in arbitrary units as a function of time at $T = 200$ K. The friction strength, $\eta/m_{\mathrm{s}}\omega_{\mathrm{b}}$, of the solid line is 0.05, the dashed line 0.3752 and the dot-dashed line 1.0. Dotted line indicates the time up to which the symmetrized correlation function data was computed by simulation and analytically continued. Note the recrossing and crossing events predicted by maximum entropy method occur after the cutoff time $\beta\hbar$. This figure was reproduced from Fig. 2 of Ref. [54].

The flux correlation function data were computed by path integral MC (PIMC) simulations by two different methods. In the first case, the symmetrized flux autocorrelation function was computed using the influence functional formalism [54], while in the second case, the explicit bath modes were used to compute the imaginary time correlation function [44]. The explicit bath modes were used for the latter to demonstrate that our approach does not require a harmonic bath approximation, but is readily applicable to a general many-body system. The coupling coefficients c_α between the reactive system and the bath were determined from the Ohmic spectral density function using the relation in Eq. (3),

$$c_\alpha^2 = \frac{2}{\pi} m_\alpha \omega_\alpha^2 \eta \mathrm{e}^{-\omega_\alpha/\omega_{\mathrm{c}}} \Delta\omega. \tag{26}$$

In Fig. 6 we show the dependence of the transmission coefficient, $\kappa = k/k_{\mathrm{TST}}$, on the damping parameter $\eta/m\omega_{\mathrm{b}}$ where k_{TST} is the classical transition state theory rate constant. These results are compared with the numerically exact calculations by Topaler and Makri [56]. The results are in very good agreement with those by Topaler and Makri over the entire range of frictions for both DW1 and DW2. In Fig. 6(a) we show the quantum transmission coefficient computed by analytic continuation of symmetrized flux autocorrelation function. Note that we only used the symmetrized flux data up to $t = \beta\hbar = 1578$ a.u. In the high friction regime, the recrossing is inhibited by the rapid dissipation due to the bath. As a result, the real-time flux autocorrelation function decays on a fast time scale ensuring that the calculation of the rate using short-time data is accurate. More importantly, the rate constants estimated through analytic continuation exhibit excellent agreement with the exact quantum results in the weak coupling regime as well, even though significant recrossing is possible under these conditions.

In view of that, it is interesting to assess the accuracy of our method for a system in which dynamic effects play more important role, i.e., which exhibits larger deviation from the quantum transition state theory. Such a system is DW2 studied by Topaler and Makri [56]. For this case we used imaginary time flux correlation data

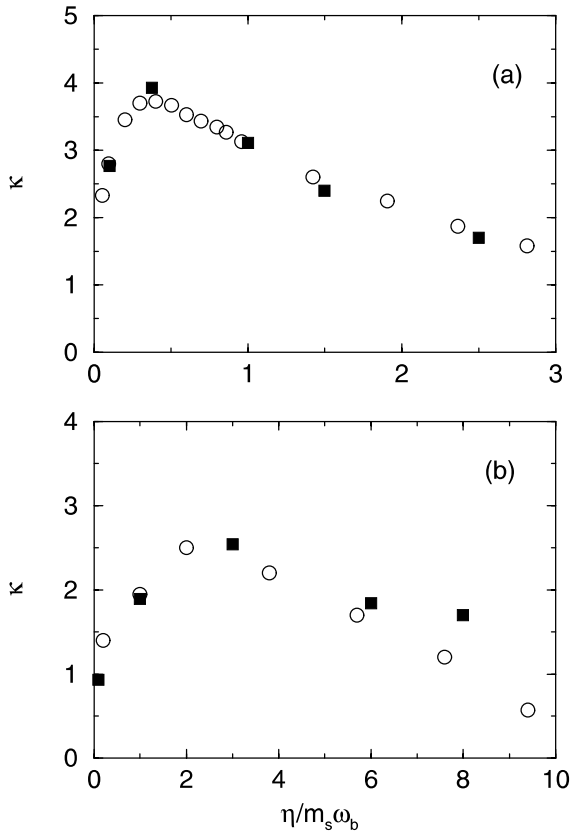

Fig. 6. Quantum transmission coefficient of proton transfer as a function of the friction strength at $T = 200$ K. (a) The case of DW1 using symmetrized flux autocorrelation data up to $t = \beta\hbar = 1578$ a.u. (b) The case of DW2 using the imaginary time flux autocorrelation data. Hollow circles are the numerically exact results from Fig. 9(b) of Ref. [56]. The results obtained by analytic continuation are shown by solid squares.

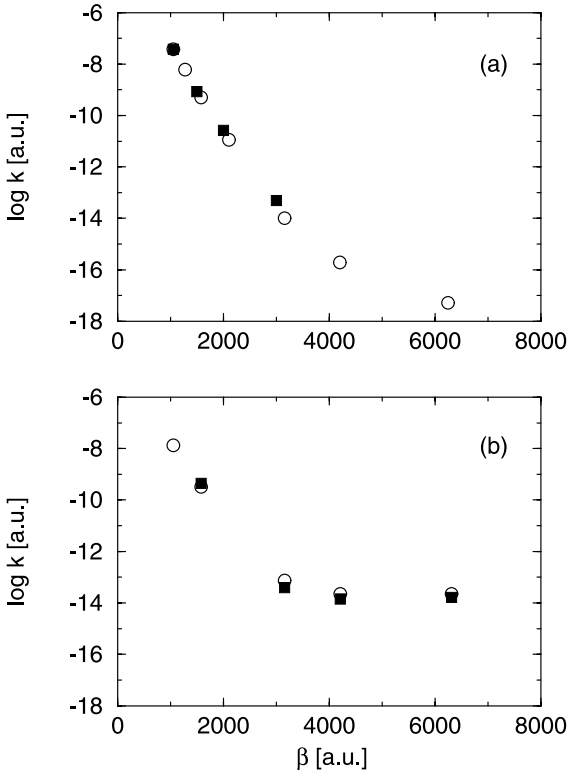

Fig. 7. The logarithm of the rate constant for DW1 as a function of inverse temperature for the friction strength, (a) $\eta/m_s\omega_b = 0.5$ and (b) $\eta/m_s\omega_b = 0.05$. The results in (a) were obtained by analytic continuation of imaginary time data, and those in (b) from the symmetrized flux autocorrelation function evaluated up to $t = \beta\hbar$ a.u. Hollow circles are the numerically exact results from Fig. 12 of Ref. [56] and the rates obtained by the method presented in this paper are shown by solid squares.

computed by PIMC using the discrete bath model [44]. The classical transmission coefficients for this case differ by almost an order of magnitude compared to their quantum mechanical counterparts [56]. The results capture the turnover in the transmission coefficient signifying the crossover from energy to spatial diffusion.

Arrhenius plots of the rate constant for DW1 [44,54] are shown in Fig. 7. The data for the turnover friction (Fig. 7(a)) were computed from imaginary time flux data [44]. At higher temperatures we obtained excellent agreement with the exact results, but at lower temperatures we were unable to converge simulation data to sufficient accuracy to allow stable inversion. For the weak friction case shown in Fig. 7(b), at the temperatures higher than the crossover temperature (estimated as $T_c \approx 100$ K), we observed a linear behavior characteristic of activated barrier crossing [54]. Conversely, at lower temperatures, tunneling dominates the dynamic process and the rate constant becomes temperature independent. Note that, in this case, the correct temperature independent tunneling rates were obtained at low temperatures as well, which additionally confirms the applicability of the analytic continuation method which includes even the deep tunneling regime.

5.2. Primary charge separation in the photosynthetic reaction center

In contrast to the typical adiabatic reaction studied in the previous section, we consider a non-adiabatic reaction in this section. The primary charge separation of photosynthesis in bacterial reaction centers involves electron transfer from an excited special chlorophyll pair (the donor) to a bacteriopheophytin of the L branch (the acceptor) [57–64]. We investigate three different types of reaction center including the wild type, a single mutant [57] and a double mutant [64].

The simplest model of non-adiabatic electron transfer is that of a discrete two state system coupled to a harmonic model of the medium. In this model, the two states, donor and acceptor, are coupled to each other as well as to a harmonic bath that describes collective modes of polarization fluctuations of the medium surrounding the reaction complex. Following the approach in Topaler and Makri [56], the flux operator is written as

$$\hat{F} = \frac{\mathrm{i}}{\hbar}[\hat{H}_{\mathrm{s}}, \hat{h}_{\mathrm{p}}] \tag{27}$$

where $\hat{H}_{\mathrm{s}}$ corresponds to the system Hamiltonian and $\hat{h}_{\mathrm{p}}$ is the product side projection operator.

In order to model the two state electron transfer, we assume that in long-distance tunneling the electronic coupling is due to superexchange. For this purpose, we used [54] McConnell's product form for the superexchange coupling matrix element [65]. The environment is described with the friction constant of the Ohmic spectral density.

The experimentally measured time constant for this particular double mutant reaction center is 20 ps [64], while the theoretically predicted time constant from the three-state reduced density matrix calculation is 21 ps [66]. Using our method the time constant obtained from the two state superexchange model was found to be 28 ps. The same result was obtained using a different spectral density obtained numerically from MD simulations by Marchi et al. [67]. The reason for this slower kinetics is the assumption of the superexchange electron transfer mechanism of two state model. It has been shown that the bridge state participates in the electron transfer resulting in a sequential electron transfer mechanism [66,68] so that the superexchange model of this study using the effective coupling of the superexchange transfer [65,69] was expected to give a slower rate, i.e., a larger time constant.

Based on the flux operator expression in Eq. (27) we also studied discrete three level system model which includes the bridge state (bacteriochlorophyll monomer) spatially located in between the donor and the acceptor. Two reaction centers are considered: the wild type and the single mutant system studied by Holten et al. [57]. The time constants that we obtained are 4.9 ps and 2.6 ps for the wild type and Holten's mutant system, respectively, while the experimentally measured time constant from both systems is 3 ps [57,62].

In brief, the analytic continuation approach appears to give accurate results for canonical rate constants for variety of reactive quantum condensed phase processes. In particular, use of the symmetrized time correlation function as an input to analytic continuation enabled us to obtain quantitatively accurate results for rate constants even in conditions of weak coupling as well as the tunneling dominated low temperature regime, which have been traditionally difficult to explore.

6. Concluding remarks

We have investigated the capabilities and limitations of the Bayesian numerical analytic continuation approach for calculating quantum time correlation functions in large anharmonic condensed phase systems. We used the method to compute the spectroscopic lineshape and the reaction rate constants in several systems described by a system-harmonic bath model. This particular model was chosen to allow comparison with the exact results, however, it should be noted that the method is not limited to such model but is rather applicable to a general many body system.

We have considered the correlation function as a function of complex time variable z. It was found that the quality of the results in some cases is affected considerably by the choice of the contour along which $C(z)$ is computed by simulations. In general, while the imaginary time contour is the

most suitable one for path integral simulations (since all the paths have real weights and therefore simulations do not suffer from the "sign problem") the analytic continuation procedure which requires one to perform an inverse Laplace transform is very unstable, thus limiting the range of accuracy of the real-time correlation function computed in this fashion to relatively short times. In contrast, computing $C(z)$ along the $z = t - i\beta\hbar/2$ contour (i.e., $G(t)$) by MC for short real-time provides for more stable inversion, however, the complex phase gives rise to the sign problem in simulations (although the sign problem is not as severe as in the case of $z = t$ contour due to cancellations of the forward and backward path phases). Nonetheless, we found that the numerical analytic continuation of $G(t)$ results in real time correlation functions that are accurate over longer time ranges provided that $G(t)$ data can be computed accurately to a sufficiently long cutoff time t_c. Fortunately, the required t_c appears to be quite short. In most cases, it appears that for cutoff time longer than $t_c \approx \beta\hbar/2$ using $G(t)$ gives superior results to use $C(-i\tau)$ alone. Hence, for example, we were able to compute the tunneling rates by the analytic continuation of the symmetrized flux autocorrelation function whereas the imaginary time data could not be calculated to sufficient accuracy to allow stable inversion in this regime.

Thus one possibility for improving the method would be to determine a complex time contour with optimal properties from both simulation and inversion stand points. For example, one may consider the contour $z = \tau(1 - i)$, $0 \leqslant \tau \leqslant \beta\hbar$, first suggested by Baym and Mermin [37].

Acknowledgements

This work was supported by a grant to BJB from the National Science Foundation.

References

[1] B.J. Berne, in: H. Eyring (Ed.), Physical Chemistry: An Advanced Treatise volume VIIIB, Academic, New York, 1971, p. 539.
[2] B.J. Alder, T.E. Wainwright, in: I. Progigine (Ed.), Proc. Int. Symp. Stat. Mech. Theory of Transport Processes, Wiley, New York, 1958, p. 97.
[3] A. Rahman, Phys. Rev. 136 (1964) A405.
[4] R.P. Feynman, Int. J. Th. Phys. 21 (1982) 467.
[5] E.J. Heller, J. Chem. Phys. 64 (1976) 63.
[6] R.B. Gerber, R.B. Buch, M.A. Ratner, J. Chem. Phys. 77 (1982) 3022.
[7] R.B. Gerber, M.A. Ratner, J. Chem. Phys. 74 (1988) 97.
[8] R.K. Preston, J.C. Tully, J. Chem. Phys. 55 (1971) 562.
[9] J.C. Tully, in: W.H. Miller (Ed.), Dynamics of Molecular Collisions, Plenum, New York, 1976.
[10] J.C. Tully, J. Chem. Phys. 93 (1990) 1061.
[11] J.C. Tully, in: B.J. Berne, G. Ciccotti, D.F. Coker (Eds.), Classical and Quantum Dynamics in Condensed Phase Simulations, World Scientific, Singapore, 1998.
[12] D.F. Coker, in: M.P. Allen, D.J. Tildesley (Eds.), Computer Simulations in Chemical Physics, Kluwer Academic, Dordrecht, 1993.
[13] W.H. Miller, J. Chem. Phys. 53 (1970) 3578.
[14] M.F. Herman, E. Kluk, Chem. Phys. 91 (1984) 27.
[15] E.J. Heller, J. Chem. Phys. 94 (1991) 2723.
[16] K.G. Kay, J. Chem. Phys. 100 (1994) 4377.
[17] F. Grossman, A.L. Xavier, Phys. Lett. A 243 (1998) 243.
[18] X. Sun, W.H. Miller, J. Chem. Phys. 110 (1999) 6635.
[19] J. Cao, G.A. Voth, J. Chem. Phys. 100 (1994) 5093.
[20] J. Cao, G.A. Voth, J. Chem. Phys. 100 (1994) 5096.
[21] J. Cao, G.A. Voth, J. Chem. Phys. 101 (1994) 6157.
[22] V.S. Filinov, Nucl. Phys. B 271 (1986) 717.
[23] J.D. Doll, D.L. Freeman, M.J. Gillan, Chem. Phys. Lett. 143 (1988) 277.
[24] J.D. Doll, D.L. Freeman, M.J. Gillan, J. Chem. Phys. 89 (1988) 5753.
[25] N. Makri, W.H. Miller, J. Chem. Phys. 89 (1988) 2170.
[26] C.H. Mak, D. Chandler, Phys. Rev. A 41 (1990) 5709.
[27] C.H. Mak, D. Chandler, Phys. Rev. A 44 (1991) 2352.
[28] M. Topaler, N. Makri, Chem. Phys. Lett. 210 (1993) 285.
[29] N. Makri, Chem. Phys. Lett. 193 (1992) 435.
[30] N. Makri, J. Chem. Phys. 97 (1993) 2417.
[31] C.H. Mak, Phys. Rev. Lett. 68 (1992) 899.
[32] R. Egger, C.H. Mak, Phys. Rev. B 50 (1994) 15210.
[33] C.H. Mak, R. Egger, J. Chem. Phys. 110 (1999) 12.
[34] R. Egger, L. Muhlbacher, C.H. Mak, Phys. Rev. E 61 (2000) 5961.
[35] R. Zwanzig, J. Stat. Phys. 9 (1973) 215.
[36] A.O. Caldeira, A.J. Leggett, Phys. Rev. Lett. 46 (1981) 211.
[37] G. Baym, D. Mermin, J. Math. Phys. 2 (1961) 232.
[38] J.E. Gubernatis, M. Jarrell, R.N. Silver, D.S. Sivia, Phys. Rev. B 44 (1991) 6011.
[39] E. Gallicchio, B.J. Berne, J. Chem. Phys. 105 (1996) 7064.
[40] E. Gallicchio, B.J. Berne, J. Chem. Phys. 101 (1994) 9909.
[41] E. Gallicchio, S.A. Egorov, B.J. Berne, J. Chem. Phys. 109 (1998) 7745.
[42] G. Krilov, E. Sim, B.J. Berne, J. Chem. Phys. 114 (2001) 1075.
[43] D. Kim, J.D. Doll, J.E. Gubernatis, J. Chem. Phys. 106 (1997) 1641.

[44] E. Rabani, G. Krilov, B.J. Berne, J. Chem. Phys. 112 (2000) 2605.
[45] D. Kim, J.D. Doll, D.L. Freeman, J. Chem. Phys. 108 (1998) 3871.
[46] B.J. Berne, G.D. Harp, Adv. Chem. Phys. XVII (1970) 63.
[47] D. Thirumalai, B.J. Berne, J. Chem. Phys. 81 (1984) 2512.
[48] J. Skilling (Ed.), Maximum Entropy and Bayesian Methods, Kluwer Academic, Dordrecht, 1989.
[49] M. Jarrell, J.E. Gubernatis, Phys. Rep. 269 (1996) 133.
[50] C.L. Lawson, R.J. Hanson, Solving Least Squares Problems, Prentice Hall, 1974.
[51] K. Miller, SIAM J. Math. Anal. 1 (1970) 52.
[52] B.J. Berne, M.E. Tuckerman, J.E. Straub, A.L.R. Bug, J. Chem. Phys. 93 (1990) 5084.
[53] J.S. Bader, B.J. Berne, J. Chem. Phys. 100 (1994) 8359.
[54] E. Sim, G. Krilov, B.J. Berne, J. Chem. Phys., in press.
[55] W.H. Miller, S.D. Schwartz, J.W. Tromp, J. Chem. Phys. 79 (1983) 4889.
[56] M. Topaler, N. Makri, J. Chem. Phys. 101 (1994) 7500.
[57] D. Holten, C. Hoganson, M.W. Windson, C.C. Schenck, W.W. Parsons, A. Migus, R.L. Fork, C.V. Shank, Biochem. Biophys. Acta 592 (1980) 461.
[58] N.W. Woodbury, M. Becker, D. Middendort, W.W. Parson, Biochemistry 24 (1985) 7516.
[59] J.L. Martin, J. Breton, A.J. Hoff, A. Migus, A. Antonetti, Proc. Natl. Acad. Sci. USA 83 (1986) 957.
[60] J. Breton, J.L. Martin, A. Migus, A. Antonetti, A. Arszag, Proc. Natl. Acad. Sci. USA 83 (1986) 5121.
[61] J. Breton, J.L. Martin, G.R. Fleming, J.-C. Lambry, Biochemistry 27 (1988) 9276.
[62] G.R. Fleming, J.L. Martin, J. Breton, Nature (London) 333 (1988) 190.
[63] C.-K. Chan, T.J. DiMagno, L.X.-Q. Chen, J.R. Norris, G.R. Fleming, Proc. Natl. Acad. Sci. USA 88 (1991) 11202.
[64] B.A. Heller, D. Holten, C. Kirmaier, Science 269 (1995) 1995.
[65] H.M. McConnell, J. Chem. Phys. 35 (1961) 508.
[66] E. Sim, N. Makri, J. Phys. Chem. B 101 (1997) 5446.
[67] M. Marchi, J.N. Gehlen, D. Chandler, M. Newton, J. Am. Chem. Soc. 115 (1993) 4178.
[68] N. Makri, E. Sim, M. Topaler, D.E. Makarov, Proc. Natl. Acad. Sci. USA 93 (1996) 3926.
[69] D.N. Beratan, J.N. Betts, J.N. Onuchic, Science 252 (1991) 1285.